Applied Catalysis B: Environmental 138–139 (2013) 434–445

Contents lists available at SciVerse ScienceDirect

Applied Catalysis B: Environmental

journal homepage: www.elsevier.com/locate/apcatb

BEA zeolite modified with iron as effective catalyst for N_2O decomposition and selective reduction of NO with ammonia

Paweł Boroń[a], Lucjan Chmielarz[a,*], Jacek Gurgul[b], Kazimierz Łątka[c], Tetsuya Shishido[d], Jean-Marc Krafft[e], Stanislaw Dzwigaj[e,f,**]

[a] Faculty of Chemistry, Jagiellonian University, Ingardena 3, 30-060 Kraków, Poland
[b] Jerzy Haber Institute of Catalysis and Surface Chemistry, Polish Academy of Sciences, Niezapominajek 8, 30-239 Kraków, Poland
[c] Marian Smoluchowski Institute of Physics, Jagiellonian University, Reymonta 4, 30-059 Kraków, Poland
[d] Department of Molecular Engineering, Kyoto University, Kyoto 615-8510, Japan
[e] UPMC Univ Paris 06, Laboratoire de Réactivité de Surface, Case 178, Site d'Ivry-Le Raphaël, 3 rue Galilée, 94200 Ivry sur Seine, France
[f] CNRS-UMR 7197, Laboratoire de Réactivité de Surface, Case 178, Site d'Ivry-Le Raphaël, 3 rue Galilée, 94200 Ivry sur Seine, France

ARTICLE INFO

Article history:
Received 18 December 2012
Received in revised form 4 March 2013
Accepted 6 March 2013
Available online 21 March 2013

Keywords:
Iron
BEA zeolite
Ammonia
N_2O decomposition
SCR of NO

ABSTRACT

BEA zeolite is modified by a two-steps postsynthesis method allowing incorporate iron atoms into the zeolite framework. Two series of the zeolite samples with aluminium (Fe_xAlSiBEA) and without aluminium (Fe_xSiBEA), containing various iron content (0.5–4.0 Fe wt.%) are obtained. For low Fe content (<2 Fe wt.%), iron is incorporated into the framework of SiBEA zeolite as a framework pseudo-tetrahedral Fe(III) as evidenced by combined used of XRD, DR UV–vis, XAS, ^{57}Fe Mössbauer and XPS investigations. In contrast, for higher iron content, the framework pseudo-tetrahedral Fe(III) and an extra-framework octahedral Fe(III) species are identified. For Fe_xAlSiBEA, significantly higher acidity than for Fe_xSiBEA is evidenced by FTIR with adsorption of CO and TPD of NH_3. Fe_xAlSiBEA and Fe_xSiBEA are found to be active and selective catalysts of N_2O decomposition and selective catalytic reduction of NO with ammonia. The highest catalytic activity in both processes are obtained for the $Fe_{4.0}$AlSiBEA sample containing iron mainly as the framework pseudo-tetrahedral Fe(III) and characterized by relatively high acidity.

1. Introduction

Nowadays, emission of nitrogen oxides into atmosphere is one of the major environmental problems. The elimination of NO_x and N_2O from flue gases emitted from stationary as well as mobile sources is still an important environmental issue [1,2]. Miscellaneous methods have been reported [3,4] for abatement of N_2O emissions, including its catalytic decomposition to N_2 and O_2, which seems to be one of the most promising methods. On the other hand, selective catalytic reduction (SCR) of NO_x with ammonia, is the most important process used for the elimination of NO_x from stationary sources [2,5,6]. This method has also been adapted for conversion of NO_x in diesel cars.

Metal containing zeolites are found to be efficient catalysts of N_2O decomposition as well as of SCR of NO_x with ammonia [7–13]. A large number of metals (Fe, Co, Ni and Cu) introduced into various zeolite structures (ZSM-5, beta, mordenite, ferrierite, A or X) have been reported [6,14–17] as catalytically active phase for both these reactions. It is generally accepted that the catalytic activity of metal containing zeolites depends on the nature of the metal, the type of zeolite matrix and the preparation method used for metal introduction [14,18,19].

The unique physicochemical properties of Fe-containing zeolites have made them the most interesting class of materials for various catalytic applications [20,21,16]. As it has been shown [1,22–26], BEA zeolites modified with iron are reported to present high catalytic activity in various processes, including SCR of NO_x as well as decomposition of N_2O. The effect of the preparation procedure on the speciation of iron and catalytic performance of Fe-BEA is still a subject of debate. Fe/ZSM-5 was reported to be suitable catalysts for SCR-NO with NH_3 as well as N_2O decomposition because of its high activity and durability [12,13]. Iron-containing ZSM-5 catalysts demonstrate high efficiency in SCR-NO when iron occurs as Fe^{3+} ions in ion-exchanged sites [27,28]. Long and Yang [12] have reported that different type of Fe species can be present in Fe-containing zeolite catalysts, but only Fe^{3+} ions in tetrahedral coordination are probably the active sites for the SCR-NO reaction (~100% NO conversion at about 673 K).

* Corresponding author at: Faculty of Chemistry, Jagiellonian University, Ingardena 3, 30-060 Kraków, Poland. Tel.: +48 12 6632006.
** Corresponding author at: UPMC Univ Paris 06, Laboratoire de Réactivité de Surface, Case 178, Site d'Ivry-Le Raphaël, 3 rue Galilée, 94200 Ivry sur Seine, France. Tel.: +33 1 44272113; fax: +33 1 2203405057.
E-mail addresses: chmielar@chemia.uj.edu (L. Chmielarz), stanislaw.dzwigaj@upmc.fr (S. Dzwigaj).

0926-3373/$ – see front matter © 2013 Elsevier B.V. All rights reserved.
http://dx.doi.org/10.1016/j.apcatb.2013.03.022

Pirngruber et al. [29] have reported that various preparation methods (CVD, IE, HT) lead to different types of iron species in ZSM-5 zeolites, but their catalytic behaviour in N_2O decomposition is qualitatively similar (~100% N_2O conversion at 770 K). Moreover, steaming increases the activity of all these catalysts, which, as it is suggested by authors, is attributed to the formation of Fe—O—Al species. This hypothesis has been recently supported by studies of Hensen et al. [30]. Comparing different types of zeolites modified with iron, it has been shown that the highest activity in N_2O decomposition is observed on dealuminated BEA [31]. Moreover, BEA zeolite containing mononuclear iron species is an efficient catalyst for the reduction of NO with ethanol or methane [23].

Although some studies focused on determination of the catalytic properties of BEA zeolite and its modification with transition metals in the N_2O decomposition and SCR of NO processes have been previously reported [22–26], the problem of the catalytic activity of different types of iron centres in zeolite, their speciation as well as the reaction mechanism over such species is still a subject of debate. A major problem is that current methods used for dispersing metals in zeolites are non selective and result in introduction of metals in the form of various species. The entanglement of the problem could be greatly reduced if well-defined catalysts with a single type of iron species could be prepared.

Thus, in the present work two-steps postsynthesis method has been used [22–26] to incorporate iron into vacant T-atom sites of framework of BEA zeolite. The method consists of: (i) creation of vacant T-atom sites by dealumination of BEA zeolite with nitric acid, and (ii) impregnation of the resulting SiBEA with aqueous $Fe(NO_3)_3$ solution. This postsynthesis method allows to obtain well-defined catalysts with mononuclear iron species as evidenced by DR UV–vis, XANES, EXAFS, Mössbauer and XPS spectroscopies.

In this paper, the catalytic activity of Fe_xAlSiBEA and Fe_xSiBEA zeolite catalysts in SCR of NO with ammonia and N_2O decomposition has been studied and the role of isolated mononuclear iron species and acidity is discussed.

2. Experimental

2.1. Catalysts preparation

Fe_xAlSiBEA and Fe_xSiBEA zeolites (x = 0.5, 1.0, 4.0 Fe wt.%) were prepared by the two-steps postsynthesis method reported earlier [1]. In the first step, 2 g of a AlBEA zeolite, obtained by calcination in air at 823 K for 15 h of tetraethylammonium BEA (TEABEA) zeolite (Si/Al = 12.5) provided by RIPP (China), was treated with a 8 or 13 mol L^{-1} HNO_3 solution under stirring (4 h, 353 K) to remove aluminium. In the second step, the resulting solids AlSiBEA (Si/Al = 100) or SiBEA (Si/Al = 1000) obtained after filtration were stirred for 24 h at room temperature in aqueous solutions (pH 2.5) containing from 0.36×10^{-3} to 1.8×10^{-2} mol L^{-1} of $Fe(NO_3)_3 \cdot 9H_2O$. The suspensions were further stirred in air at 353 K for 2 h until complete evaporation of water. The solids with 0.5, 1.0 and 4.0 Fe wt.% were labelled $Fe_{0.5}$AlSiBEA, $Fe_{1.0}$AlSiBEA and $Fe_{4.0}$AlSiBEA or $Fe_{0.5}$SiBEA, $Fe_{1.0}$SiBEA and $Fe_{4.0}$SiBEA, respectively.

2.2. Catalysts characterization

X-ray fluorescence chemical analysis was performed at room temperature on a SPECTRO X-LabPro apparatus.

The structure of studied materials was determined by powder X-ray diffraction. Powder X-ray diffraction patterns of the materials were measured in a PW 3710 Philips X'pert (Philips X'pert APD) using Ni-filtered Cu Kα radiation (λ = 1.54056 Å) in the range of 2Θ from 5° to 50° with a 0.02° step.

Specific surface area and adsorption isotherms of nitrogen at 77 K were measured on a Micromeretics ASAP 2010 apparatus. All samples were outgassed, first at room temperature, then at 623 K to a pressure < 0.2 Pa. The specific surface areas were determined from nitrogen adsorption values for five relative pressure (P/P_0) ranging from 0.05 to 0.16 using BET method. The microporous pore volume was determined from the amount of N_2 adsorbed up to P/P_0 = 0.2.

The structure of the obtained materials on microscopic level was studied by IR spectroscopy. FTIR spectra were recorded by DRIFT measurements performed with a Nicolet 6700 Thermo Scientific spectrometer. A sample was ground with KBr (1 wt.%). 200 scans were collected in the range of 600–4000 cm^{-1} with 4 cm^{-1} resolution.

The DR UV–vis spectra were recorded using an Evolution 600 (Thermo) spectrophotometer. The measurements were performed in the range of 200–600 nm with a resolution of 2 nm. DR UV–vis spectroscopy was applied to determine chemical nature of the Fe species in zeolite structure.

X-ray absorption spectra (XAS) are measured on the beam line BL11 at SAGA light source Kyushu Synchrotron Light Research Centre at SAGA, Japan. Fe K-edge XANES and EXAFS are measured with a transmission mode at room temperature using two ion chambers. Si(111) single crystal is used to obtain a monochromatic X-ray beam. Analysis of EXAFS data is performed using the REX2000 programme (Version: 2.5.9; Rigaku Corp.). The oscillation is normalized by the edge height around 70–100 eV higher than the threshold. The Fourier transformation of k^3-weighted EXAFS oscillation is performed over a k-range of 3.5–13.5 $Å^{-1}$.

The ^{57}Fe Mössbauer spectra were measured at room temperature employing the 14.4 keV gamma resonance transition. A Mössbauer system that consists of the Janis top loaded liquid helium cryostat (Janis Research Company, Wilmington, MA 01887, USA) integrated with a conventional constant-acceleration spectrometer (Science Engineering & Education Co., USA) of the Kankeleit type in transmission geometry was used. During measurements, 100 mCi Mössbauer ^{57}Co(Rh) γ-ray source and the absorbers were kept at room temperature. The absorbers were made of the fine powdered materials placed in a thin-walled (~0.1 mm) cylindrical plastic container. The absorber thicknesses of about 109–133 mg/cm^2 were calculated from the optimization procedure [32]. The resonance 14.4 keV gamma rays (for a given measurement and the energy scale calibration) were detected simultaneously by means of two independent LND Kr/Co_2 proportional gas counters attached at opposite sides of the driving system. The drive velocity calibration was performed with a second ^{57}Co(Rh) source against a standard metallic iron foil at room temperature. It is worth noting that the usage of Mössbauer technique for the samples under study was rather time consuming, in spite of the fact that our source was relatively strong, since to get a reasonable good quality of Mössbauer spectrum required up to two weeks of measuring period, especially in the case of the sample with low content of iron.

The ^{57}Fe Mössbauer spectra were analyzed numerically by fitting a hyperfine parameter distribution (HPD) using the Voigt-line-based method of Rancourt and Ping [33]. In this method, the HPD for a given crystal site corresponding to similar structural, chemical and magnetic properties is constructed by a sum of Gaussian components for the quadrupole splitting (QS) distributions and, if necessary, the magnetic hyperfine field B_{hf} distributions. The isomer shift (IS) was linearly coupled to the primary hyperfine parameters (QS, B_{hf}).

The X-ray photoelectron spectroscopy (XPS) measurements were carried out with a hemispherical analyzer (SES R4000, Gammadata Scienta, pass energy 100 eV). The unmonochromatized AlK_α X-ray source (1486.6 eV, 11 kV, 17 mA) without a charge neutralizer was applied to generate core excitation. The system was

calibrated according to ISO 15472:2001. The energy resolution of the system, measured as a full width at half maximum (FWHM) for Ag $3d_{5/2}$ excitation line, was 0.9 eV. The powder samples were pressed into indium foil and mounted on a dedicated holder and then UHV evacuated. During the measurements, the base pressure in the analysis chamber was about 10^{-9} mbar. The area of the sample analysis was approximately 3 mm^2. All binding energy (BE) values were charge-corrected to the carbon C 1s excitation set at 285.0 eV. The Shirley-type background subtraction was used to the spectra prior to the fitting procedure, where Voigt line shape, i.e. Gaussian/Lorentzian functional (70:30) was applied. The Fe 2p core excitations were deconvoluted with a relative intensity ratio of $2p_{3/2}$ and $2p_{1/2}$ lines fixed to 2:1.

The acidity of AlSiBEA and SiBEA supports was investigated by FTIR using CO as a probe molecule. Before CO adsorption experiment, the wafers of AlSiBEA and SiBEA were activated by calcination at 723 K for 2 h in a flow of 2.5 vol.% of O_2 diluted in Ar and then outgassed at 573 K (10^{-3} Pa) for 1 h. Following thermal treatment, the samples were cooled down to 100 K. CO was introduced in increasing amounts up to an equilibrium pressure of 133 Pa. Infrared spectra were recorded using a Bruker Vertex 70 spectrometer (resolution of 2 cm^{-1}, 128 scans). The spectra were obtained after subtraction of the spectrum recorded after calcination and prior to CO adsorption.

The acidity (concentration and strength of acidic sites) of Fe_xAlSiBEA and Fe_xSiBEA was also investigated by temperature programmed desorption of ammonia (TPD of NH_3). The TPD of NH_3 measurements was carried out in the temperature range of 343–923 K in a fix bed continuous flow microreactor. The reaction temperature was measured by a K-type thermocouple located in a quartz capillary immersed in the catalyst bed. The molecules desorbing from the zeolite samples were monitored on line by a quadrupole mass spectrometer (VG Quartz) connected directly to the reactor outlet via a heated line. Before TPD of NH_3 experiments, the zeolite sample (100 mg) was outgassed in a flow of pure helium (20 ml/min) at 773 K for 1 h. Subsequently, the sample was cooled down to 373 K and saturated for about 30 min in a flow of 1 vol.% of NH_3 diluted in He (20 mL^{-1} min). Then the catalyst was purged in a flowing pure helium until a constant baseline level was attained. Desorption was carried out with the linear heating rate (10 K/min) in a flowing pure helium (20 mL^{-1} min). Calibration of the quadrupole mass spectrometer with commercial mixtures allowed to recalculate the detector signal into a desorption rate.

2.3. Catalytic tests

$Fe_{0.5}$AlSiBEA, $Fe_{1.0}$AlSiBEA and $Fe_{4.0}$AlSiBEA as well as $Fe_{0.5}$SiBEA, $Fe_{1.0}$SiBEA and $Fe_{4.0}$SiBEA were investigated as catalysts for N_2O decomposition and SCR of NO with ammonia.

2.3.1. Catalytic decomposition of N_2O

The catalytic tests were performed in a plug flow microreactor system. The catalyst sample (100 mg) was loaded at the central position of the reactor onto a quartz wool plug. The flow of the gaseous reactants was kept at 50 mL^{-1} min using mass flow controllers (Brooks 5850E). The reaction products were monitored by a SRI 8610C gas chromatograph (equipped with two capillary columns-Hayesep-D, Molsieve-5A and TCD detector. Prior to the catalytic run the sample was outgassed at 723 K in a flow of pure helium. The dosing reaction mixture containing: $[N_2O]$ = 0.5 vol.%, $[O_2]$ = 4.5 vol.% and [He] = 95 vol.% was started immediately after outgassing process. Temperature of the reactor was increased from 423 to 873 K in steps of 50 K. The first GC analysis at each selected temperature was performed after 15 min since the reactor temperature was stabilized.

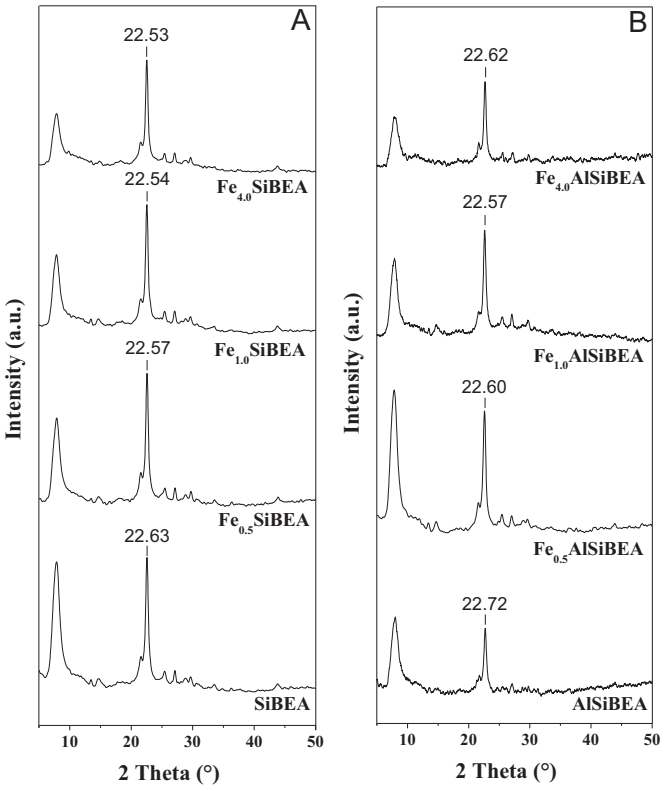

Fig. 1. XRD patterns recorded at room temperature of SiBEA, $Fe_{0.5}$SiBEA, $Fe_{1.0}$SiBEA, $Fe_{4.0}$SiBEA (A) and AlSiBEA, $Fe_{0.5}$AlSiBEA, $Fe_{1.0}$AlSiBEA, $Fe_{4.0}$AlSiBEA (B).

2.3.2. SCR of NO with ammonia

Catalytic experiments were performed in a fixed-bed flow microreactor system. The reactant concentrations were continuously measured using a quadrupole mass spectrometer (VG Quartz) connected directly to the reactor outlet. Prior to the reaction, each sample (100 mg) of the catalyst was outgassed in a flow of pure helium at 823 K for 30 min. The following composition of the gas mixture was used: [NO] = [NH3] = 0.25 vol.%, [O2] = 2.5 vol.% and [He] = 97 vol.%.

3. Results and discussion

3.1. Crystallinity and textural properties of studied materials

Fig. 1 presents X-ray diffraction patterns of SiBEA, $Fe_{0.5}$SiBEA, $Fe_{1.0}$SiBEA, $Fe_{4.0}$SiBEA (Fig. 1A) and AlSiBEA, $Fe_{0.5}$AlSiBEA, $Fe_{1.0}$AlSiBEA and $Fe_{4.0}$AlSiBEA (Fig. 1B). The XRD patterns of all samples are similar and characteristic of BEA zeolite. The absence of diffraction reflections related to extra-framework phases in the samples indicates a good dispersion of iron. The similar XRD diffractograms of all samples show that dealumination of TEABEA zeolite as well as introduction of iron ions into SiBEA and AlSiBEA do not induce any significant changes in the BEA structure. The characteristic increase of the d_{302} spacing from 3.925 Å (2Θ = 22.63°) for SiBEA to 3.943 Å (2Θ = 22.53°) for $Fe_{4.0}$SiBEA upon introduction of 4.0 wt.% of Fe into SiBEA (Fig. 1A) indicates expansion of the matrix as a result of the reaction of iron ions with OH groups of vacant T-atom sites (T = Si or Al) and their incorporation into the framework positions of BEA zeolite, as reported earlier [2].

The introduction of iron ions in AlSiBEA zeolite by postsynthesis method leads to an increase of the interlayer distance from 3.910 Å (2Θ = 22.72°) for AlSiBEA to 3.936 Å (2Θ = 22.57°) for $Fe_{1.0}$AlSiBEA (Fig. 1B). The progressive shift of the characteristic (302) reflection to lower values of 2Θ angles with increasing content of iron

can be related to the introduction of iron into the framework of BEA zeolite. In contrast, the introduction of 4.0 wt.% of iron into AlSiBEA zeolite does not lead to a such significant increase in the d_{302} spacing as for the $Fe_{1.0}$AlSiBEA sample (3.927 Å, $2\Theta = 22.62^{\circ}$) suggesting that only some amounts of iron has been incorporated into the framework of BEA zeolite. Moreover, X-ray diffractogram recorded for each sample contains (3 0 2) reflection having similar intensity, suggesting that the incorporation of iron into zeolite precursor does not affect their crystallinity.

Nitrogen adsorption–desorption isotherms of SiBEA, Fe_xSiBEA, AlSiBEA and Fe_xSiBEA samples may be classified as type I according to IUPAC. They are very similar to each other (results not shown). Moreover, all these materials have similar BET surface area (490–530 $m^2\ g^{-1}$) and micropore volume (0.23–0.25 $cm^3\ g^{-1}$) characteristic for the BEA structure indicating that textural properties of BEA zeolite are preserved upon dealumination and incorporation of iron into the framework of both SiBEA and AlSiBEA samples.

3.2. FTIR evidence of iron incorporation in the framework of SiBEA and AlSiBEA zeolite

Dealumination of BEA zeolite induces a significant shift of the band corresponding to the υ_{As}(Si—O) vibrations, known to be sensitive to the chemical composition of zeolite. Band observed at 1093 cm^{-1} for AlSiBEA (Fig. 2B), characteristic of υ_{As}(Si—O) vibration, is shifted to 1098 cm^{-1} for SiBEA (Fig. 2A).

While the bands near 960 cm^{-1} (FeSiBEA) and 950 cm^{-1} (FeAlSiBEA) can be attributed to the presence of a large amount of silanol groups in the samples. These bands, already observed for various siliceous zeolites [34], have been assigned to the stretching vibration of Si—O belonging to uncoupled (SiO_4) tetrahedra with hydroxyl group. The band found in the range of 950–970 cm^{-1} confirms the presence of vacant T-sites associated with silanol groups, generated upon dealumination of the BEA zeolite framework. The bands detected at 964 and 952 cm^{-1} for Fe_xSiBEA and Fe_xAlSiBEA, respectively, are usually assigned to Si—O(H) stretching vibration. It should be noted that these bands disappeared after introduction of higher amount of iron into BEA zeolite (Fig. 2A and B). This effect is more significant for ~~a~~ FeAlSiBEA and can be related to the incorporation of iron into vacant T-sites.

As it was shown earlier [2,35], the FTIR spectrum of BEA zeolite exhibits some characteristic bands due to the hydroxyl stretching modes of AlO–H groups at 3665 cm^{-1}, ≡Al(III)—O(H)—Si≡ groups at 3609 cm^{-1}, isolated SiO–H groups at 3740 cm^{-1} and H-bonded SiO–H groups at 3520 cm^{-1}.

The FTIR spectra of AlSiBEA and SiBEA after dealumination are shown in Fig. 3. It can be seen that there are some differences between both materials: AlSiBEA (Si/Al = 100) exhibits five well resolved bands at 3750, 3743, 3715, 3630 and 3490 cm^{-1}, whereas SiBEA (Si/Al = 1000) four bands at 3750, 3739, 3715 and 3520 cm^{-1} due to isolated external, isolated internal, terminal internal and hydrogen bonded SiO—H located in vacant T-atom sites forming hydroxyl nests (Fig. 3). These results are in line with assignments reported earlier [7,8,13,14]. The bands at 3630 and 3490 cm^{-1} appear in the spectrum of partially dealuminated AlSiBEA and correspond to ≡Al(III)—O(H)—Si≡ and hydrogen bonded SiO—H groups.

The incorporation of Fe into AlSiBEA and SiBEA, leading to Fe_xAlSiBEA and Fe_xSiBEA, induces a reduction of the intensity of the bands characteristics of hydroxyl nests and in particular bands at 3715 and 3490–3520 cm^{-1} corresponding to terminal internal and hydrogen bonded SiO—H groups as shown in Fig. 3 for $Fe_{4.0}$AlSiBEA and $Fe_{4.0}$SiBEA. It suggests that SiO—H groups of hydroxyl nests reacts with Fe ions with formation of framework pseudo-tetrahedral Fe(III) species. It is confirmed by a small increasing and broadening of the intensity of the FTIR band at 3630 cm^{-1} for $Fe_{4.0}$AlSiBEA and appearance of the band at

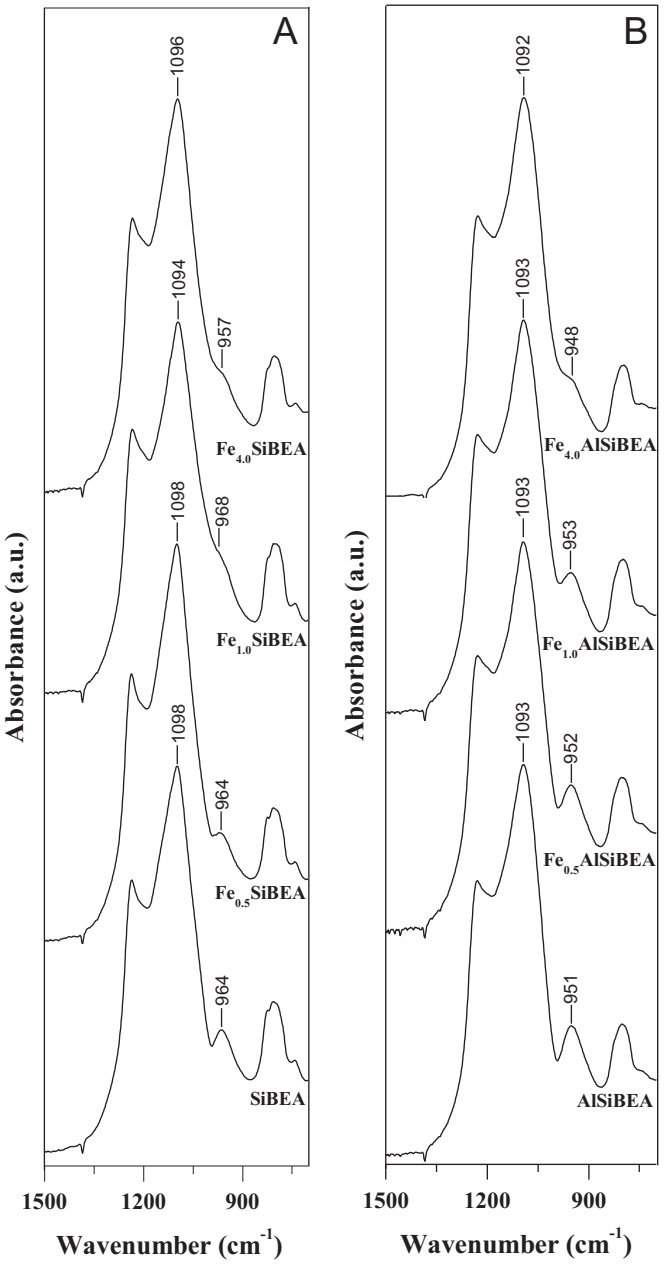

Fig. 2. FTIR spectra (KBr) recorded at room temperature of SiBEA, $Fe_{0.5}$SiBEA, $Fe_{1.0}$SiBEA, $Fe_{4.0}$SiBEA (A) and AlSiBEA, $Fe_{0.5}$AlSiBEA, $Fe_{1.0}$AlSiBEA, $Fe_{4.0}$AlSiBEA (B).

3630 cm^{-1} for $Fe_{4.0}$SiBEA attributed to ≡Fe(III)—O(H)—Si≡ acidic sites. The similar phenomenon has earlier been observed upon incorporation of chromium into SiBEA zeolite, what resulted in the formation of ≡Cr(III)—O(H)—Si≡ acidic sites [36].

3.3. Nature and environment of the iron in Fe_xSiBEA and Fe_xAlSiBEA.

The nature and environment of iron present in Fe_xSiBEA and Fe_xAlSiBEA materials have been studied by DR UV–vis, XAS, Mössbauer and XPS spectroscopies. Fig. 4 shows the results of DR UV–vis obtained for $Fe_{0.5}$SiBEA, $Fe_{1.0}$SiBEA, $Fe_{4.0}$SiBEA, $Fe_{0.5}$AlSiBEA, $Fe_{1.0}$AlSiBEA and $Fe_{4.0}$AlSiBEA. The DR UV–vis spectra for the samples with low iron content (0.5, 1.0 wt.%) contain a peak centred at about 253–276 nm assigned to oxygen-to-metal charge transfer transition involving framework pseudo-tetrahedral Fe(III) species [22,26,37–43]. The absence of a broad band near 500 nm

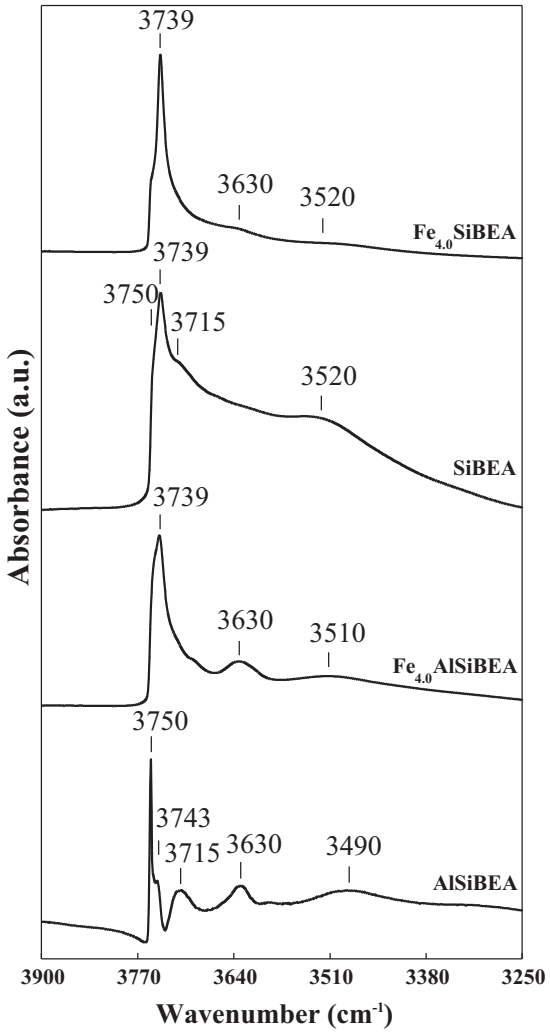

Fig. 3. FTIR spectra recorded at room temperature of SiBEA, $Fe_{4.0}$SiBEA, AlSiBEA and $Fe_{4.0}$AlSiBEA in the range of vibration of OH groups.

suggests that FeO_x oligomers are not present [37–39]. It should be noted that upon preparation of these samples by two-step post-synthesis method almost all iron has been incorporated into the zeolite framework and therefore, all these samples are white.

For the samples with higher iron content ($Fe_{4.0}$SiBEA, $Fe_{4.0}$AlSiBEA), much more intense bands at 270–278 nm assigned to framework pseudo-tetrahedral Fe(III) and additionally a band at 339–343 nm attributed to extra-framework octahedral Fe(III) species are observed [16]. The presence of a small amount of extra-framework octahedral Fe(III) species is confirmed by the light brown colour of these samples.

Fig. 5(left side) shows the Fe K-edge XANES spectra of reference compounds (ferrisilicate and α-Fe_2O_3) and of $Fe_{0.5}$SiBEA, $Fe_{1.0}$SiBEA, $Fe_{2.0}$SiBEA and $Fe_{4.0}$SiBEA. Fe species are tetrahedral in ferrisilicate and octahedral in α-Fe_2O_3. The pre-edge peak at ~7114 eV, assigned to the 1s–3d dipolar transition, is sensitive to the electronic and geometric structures of iron. This forbidden transition generally gains intensity when Fe ion loses its inversion centre upon temperature-dependent distortion or it is tetrahedral (mixing of 3d and 4p orbitals). Although, the intensity of this pre-edge peak is expected to increase as follows: $I_{\text{octahedral}} < I_{\text{square pyramidal}} < I_{\text{tetrahedral}}$ (Fig. 5) [44,45], it is weak, even for tetrahedral Fe(III) species.

Ferrisilicate, with tetrahedral Fe(III) species, exhibits the highest intensity, whereas α-Fe_2O_3 with distorted octahedral Fe(III) ions exhibits a very weak and broad absorption. The pre-edge peak intensity for $Fe_{0.5}$SiBEA, $Fe_{1.0}$SiBEA, $Fe_{2.0}$SiBEA and $Fe_{4.0}$SiBEA samples is lower than that for ferrisilicate, and higher than that for α-Fe_2O_3. The oscillations observed for Fe_xSiBEA at high energy (about 15 eV above the absorption edge) are different than that of ferrisilicate. It confirms difference in local structure of Fe in both zeolite systems. In ferrisilicate, FeO_4 units with four Fe—O bonds with the same Fe—O length are present. In contrast, in the Fe_xSiBEA sample FeO_4 units are present but with different Fe—O length. It suggests that in Fe_xSiBEA Fe(III) in pseudo-tetrahedral or higher coordination are present, in contrast to ideal tetrahedral Fe(III) species occurred in ferrisilicate. Moreover, it seems that Fe—O bonds in Fe_xSiBEA are longer than that in ferrisilicate. Above-mentioned results evidence that iron in $Fe_{0.5}$SiBEA, $Fe_{1.0}$SiBEA,

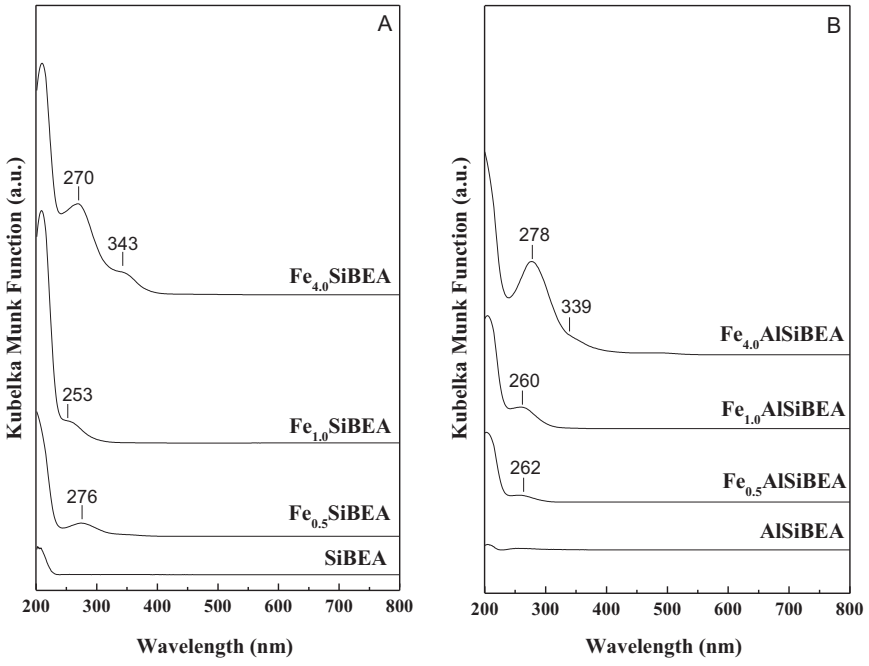

Fig. 4. DR UV–vis spectra recorded at ambient atmosphere of SiBEA, $Fe_{0.5}$SiBEA, $Fe_{1.0}$SiBEA, $Fe_{4.0}$SiBEA (A) and AlSiBEA, $Fe_{0.5}$AlSiBEA, $Fe_{1.0}$AlSiBEA, $Fe_{4.0}$AlSiBEA (B).

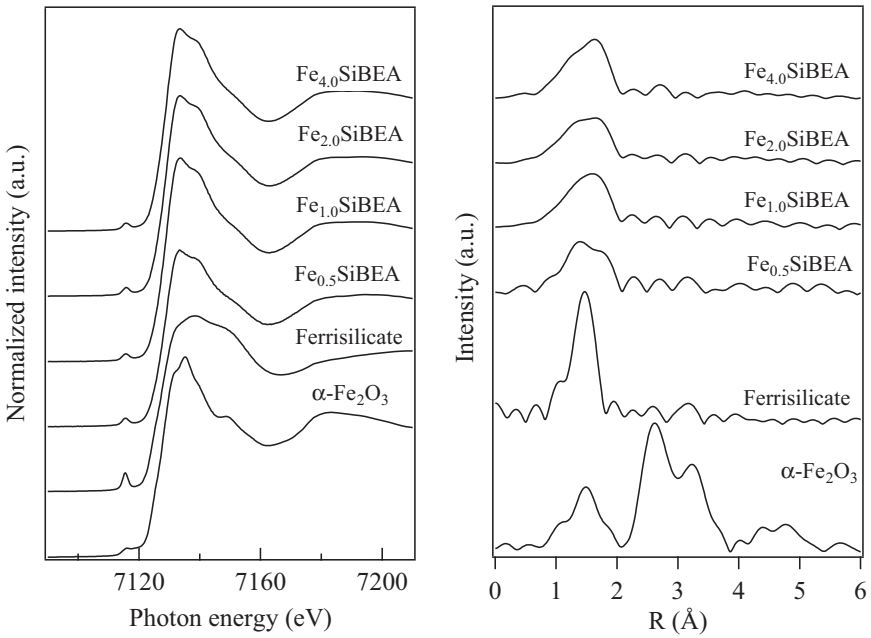

Fig. 5. XANES spectra (left side) and Fourier transforms (FTs) (right side) recorded at room temperature of α-Fe_2O_3 and ferrisilicate references and $Fe_{0.5}$SiBEA, $Fe_{1.0}$SiBEA, $Fe_{2.0}$SiBEA and $Fe_{4.0}$SiBEA.

$Fe_{2.0}$SiBEA and $Fe_{4.0}$SiBEA is mainly present as Fe(III) in pseudo-tetrahedral or higher coordination.

Fig. 5(right side) shows also Fourier transforms (not phase shift-corrected) of reference compounds (ferrisilicate and α-Fe_2O_3) and $Fe_{0.5}$SiBEA, $Fe_{1.0}$SiBEA, $Fe_{2.0}$SiBEA and $Fe_{4.0}$SiBEA samples. Two peaks at about 1.5–1.7 Å can be assigned to the two contributions of the Fe—O shell. It should be noted that Fe···Fe interactions detected in α-Fe_2O_3 at about 2.8 Å, are not observed in $Fe_{0.5}$SiBEA, $Fe_{1.0}$SiBEA, $Fe_{2.0}$SiBEA and $Fe_{4.0}$SiBEA samples and ferrisilicate, suggesting that mainly isolated mononuclear Fe(III) species are present in all these zeolite materials.

The ^{57}Fe Mössbauer spectra of $Fe_{1.0}$SiBEA, $Fe_{4.0}$SiBEA, $Fe_{1.0}$AlSiBEA and $Fe_{4.0}$AlSiBEA were collected at room temperature and their fitted parameters are reported in Figs. 6 and 7 as well as in Table 1, respectively. The spectra of the samples with low Fe content, $Fe_{1.0}$SiBEA and $Fe_{1.0}$AlSiBEA, show two dominant doublets with low isomer shift values ($0.18 \leq IS \leq 0.23$ mm s^{-1}) which are characteristic of iron Fe(III) species in pseudo-tetrahedral surroundings, what is in line with our previous study [46]. The observed quadrupole splitting values QS are rather modest suggesting less distorted charge distribution around the framework iron species. In the $Fe_{1.0}$SiBEA sample additional component (almost 9% of total area) is visible. A very small IS of this component corresponds to the Fe^{4+} species according to results published recently [47]. Some traces of Fe^{4+} species are also seen in the spectra of $Fe_{4.0}$SiBEA and $Fe_{4.0}$AlSiBEA with high amount of iron. The ^{57}Fe Mössbauer signal with a higher value of IS and quite large value of QS can be attributed to the Fe(III) species in the octahedral surroundings (Table 1). Moreover, very high values of QS (>2 mm s^{-1}) can be tentatively prescribed to the iron ions in the extra-framework (EFW) positions or to the adjacent iron ions near to defect sites such as $(SiO)_2$—Fe^{3+}—O—Fe^{3+}—(OH)(OSi) [48].

In spite of some differences, one can note that all the samples (containing iron with natural abundance) show no traces of Fe(II). Moreover, lack of magnetic sextets excludes the presence of magnetic oxides, i.e. Fe_2O_3 and/or Fe_3O_4 in our zeolites proving a good quality of the prepared samples. Over 80% of iron in $Fe_{1.0}$SiBEA, $Fe_{4.0}$SiBEA and $Fe_{4.0}$AlSiBEA is present as pseudo-tetrahedral Fe(III). It is confirmed by the fact that both components of pseudo-tetrahedral Fe(III) (with high and low QS) are characterized by a rather low Gaussian width of the QS distribution σ, which means that iron Fe(III) species are located in well-defined

Table 1
Hyperfine parameters derived from the room-temperature ^{57}Fe Mössbauer spectra for $Fe_{1.0}$SiBEA, $Fe_{4.0}$SiBEA, $Fe_{1.0}$AlSiBEA and $Fe_{4.0}$AlSiBEA. Isomer shift (IS) is given in mm s^{-1} relative to α-Fe foil. $\langle QS\rangle = e^2qQ/2$ (in mm^{-1}) and σ (in mm s^{-1}) are the average quadrupole splitting and the Gaussian width of the *QS* distribution of the given spectral component, respectively.

Sample	$\langle QS\rangle$ (mm s^{-1})	σ (mm s^{-1})	IS (mm s^{-1})	Area (%)	Site
$Fe_{1.0}$SiBEA	0.65	0.15	0.18	84.1	$Fe^{3+}(T_d)$
	1.48	0.16	0.23	6.6	$Fe^{3+}(T_d)$
	0.08	0.21	0.05	9.3	Fe^{4+}
$Fe_{4.0}$SiBEA	0.58	0.07	0.30	91.5	$Fe^{3+}(T_d)$
	0.01	0.01	0.03	4.5	Fe^{4+}
	2.37	0.87	0.54	4.0	$Fe^{3+}(O_h)$-EFW
$Fe_{1.0}$AlSiBEA	0.35	0.13	0.21	32.6	$Fe^{3+}(T_d)$
	0.98	0.23	0.20	30.8	$Fe^{3+}(T_d)$
	1.10	0.36	0.53	22.0	$Fe^{3+}(O_h)$
	2.73	0.40	0.42	14.6	$Fe^{3+}(O_h)$-EFW
$Fe_{4.0}$AlSiBEA	0.46	0.10	0.30	88.0	$Fe^{3+}(T_d)$
	1.69	0.50	0.34	5.5	$Fe^{3+}(O_h)$
	0.01	0.01	0.10	6.5	Fe^{4+}

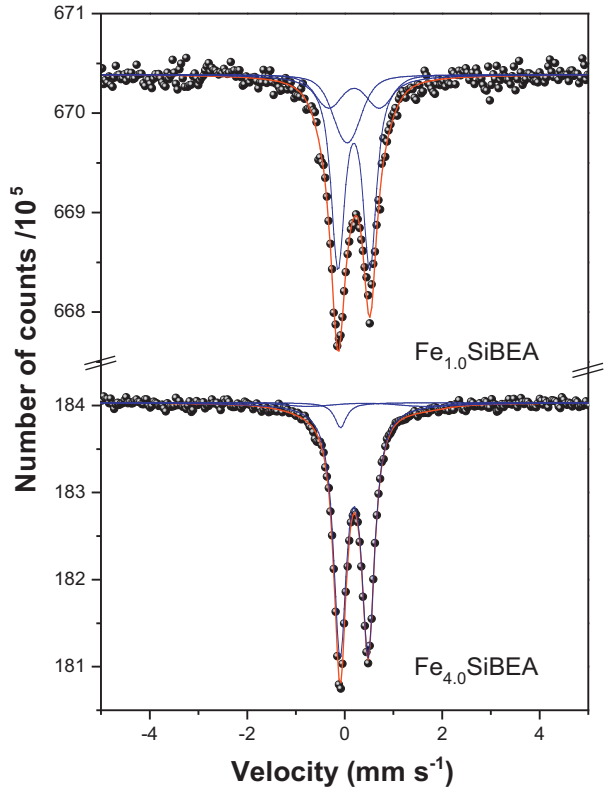

Fig. 6. Room temperature ^{57}Fe Mössbauer spectra of $Fe_{1.0}$SiBEA and $Fe_{4.0}$SiBEA.

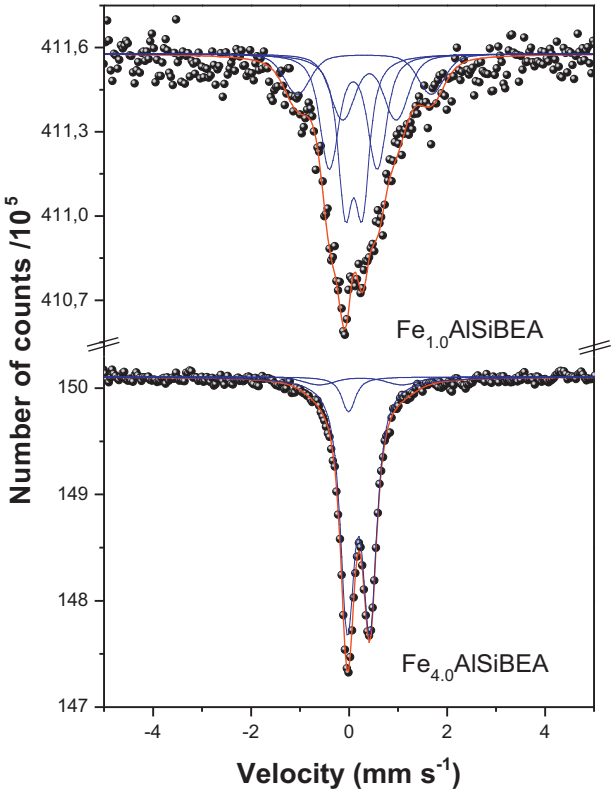

Fig. 7. Room temperature ^{57}Fe Mössbauer spectra of $Fe_{1.0}$AlSiBEA and $Fe_{4.0}$AlSiBEA.

crystallographic positions with low amount of defects. $Fe_{1.0}$AlSiBEA zeolite is a slightly different, because in this sample only 63% of iron was present in the form of pseudo-tetrahedral Fe(III) species. The rest is composed of Fe(III) species in the octahedral surroundings, what is probably related to the preparation procedure and accessibility of vacant T-atom sites during incorporation of iron ions into the zeolite framework. The careful analysis reveals also that the signal to noise ratio in $Fe_{1.0}$AlSiBEA is very poor. It leads to the conclusion that smaller amount of iron were incorporated successfully into the zeolite matrix in comparing to the $Fe_{1.0}$SiBEA sample.

XP spectra of $Fe_{1.0}$SiBEA, $Fe_{4.0}$SiBEA, $Fe_{1.0}$AlSiBEA and $Fe_{4.0}$AlSiBEA have been analyzed numerically in the BE regions of Si 2p, O 1s, C 1s and Fe 2p. Only Fe 2p spectra are presented in Supporting Information Figs. I and II.

The Si $2p_{3/2}$ BE values (103.6–103.9 eV) found in $Fe_{1.0}$SiBEA, $Fe_{4.0}$SiBEA, $Fe_{1.0}$AlSiBEA and $Fe_{4.0}$AlSiBEA are close to those reported earlier for BEA, MFI and MOR zeolites and are related to the presence of tetrahedral Si(IV) [43,49–53]. For $Fe_{1.0}$AlSiBEA and $Fe_{4.0}$AlSiBEA, a small additional component was found at lower BE (100.3–100.5 eV), which is probably related to Si present in Si—O(H)—Al groups. The O 1s lines can be well decomposed into three components: a main peak at 533.0–533.3 eV (assigned to oxygen in the zeolite framework [54]), a much smaller peak at 530.2–530.8 eV due to oxygen–metal bonds and a peak at 534.1–534.6 eV assigned to adsorbed water and/or oxygen of organic contaminants. The C 1s core lines generally consist of three peaks at 285.0 eV (organic contaminants), 286.5–286.7 eV (C—O groups) and 288.3–289.1 eV (C═O groups).

Fe 2p core level is splitted into Fe $2p_{3/2}$ and $2p_{1/2}$ doublet structure (two peaks) due to the spin–orbit coupling (Supporting Information, Figs. I and II). The Fe $2p_{3/2}$ and Fe $2p_{1/2}$ binding energies are strongly related to the iron states [55–60]. Moreover, it is well known that Fe(III) as well as Fe(II) core line is associated with shake-up satellite which is also sensitive to the Fe oxidation state [57,61]. The satellites are usually clearly distinguished (significant broadening on the high BE side of the Fe 2p photoelectron peaks), unfortunately they overlap the Fe $2p_{3/2}$ and Fe $2p_{1/2}$ lines. Sometimes, the satellites can be cancelled as it was reported for Fe_3O_4 [56,58,62] but this is not our case. It is worth noting that all these features can be used for qualitative analysis of the Fe states, although the results should be treated with some doubt. Taking into account all above-mentioned comments, our XP Fe 2p spectra of $Fe_{1.0}$SiBEA, $Fe_{4.0}$SiBEA, $Fe_{1.0}$AlSiBEA and $Fe_{4.0}$AlSiBEA have been well described by two components and associated satellites (Supporting Information, Figs. I and II). Due to poor signal to noise ratio, only one broad satellite was used in the fitting procedure.

At first sight, XP spectra of Fe_xSiBEA and Fe_xAlSiBEA with the same Fe content look quite similar, although there are several significant differences. First of all, there is a noticeably BE shift of $Fe_{1.0}$AlSiBEA iron peaks to higher binding energies in comparison to $Fe_{1.0}$SiBEA zeolite. In contrast, samples with higher content of iron do not show this relationship. In addition to the differences in binding energies, the values of the spin–orbit splitting Δ_{SO} for the above-mentioned systems also differ (Table 2). All spin–orbit splittings are larger in Fe_xAlSiBEA systems (Δ_{SO} = 13.2–14.6 eV) then in Fe_xSiBEA systems (Δ_{SO} = 12.0–13.3 eV). This indicates that Δ_{SO} values reflect not only the formal valence state of Fe but also delocalization of valence electrons, ligand field symmetry or its strength [63]. Moreover, the shake up satellites are much higher in Fe_xAlSiBEA spectra. The positions of satellites are quite similar, although their very low BE could be erroneous interpreted as coming from Fe(II) species, which is excluded by ^{57}Fe Mössbauer results.

All above-mentioned differences lead to the conclusion that dealumination process strongly influences local electronic structure of measured samples. It is worth noting that the amount

Table 2
The BE values (eV) and relative areas of components (%) of Fe 2p core excitation obtained for $Fe_{1.0}$SiBEA, $Fe_{4.0}$SiBEA, $Fe_{1.0}$AlSiBEA and $Fe_{4.0}$AlSiBEA.

Core excitation	$Fe_{1.0}$SiBEA		$Fe_{4.0}$SiBEA		$Fe_{1.0}$AlSiBEA		$Fe_{4.0}$AlSiBEA	
	BE (eV)	Area (%)	BE (eV)	Area (%)	BE (eV)	Area (%)	BE (eV)	Area (%)
Fe $2p_{3/2}$	710.3	54.6	711.0	72.8	710.8	49.9	710.9	64.1
	712.4	45.4	713.9	27.2	712.6	50.1	712.7	35.9
Fe $2p_{1/2}$	722.4		724.2		723.6		724.5	
	724.4		727.2		726.0		727.3	
Satellites	715.6		716.8		715.7		715.7	
	727.1		730.7		729.9		730.8	

of loaded iron also modify XP spectra. Generally speaking, samples with higher Fe content have higher BE and larger spin–orbit splittings, which is better visible in Fe_xSiBEA series. On the other hand, almost all binding energies of Fe $2p_{3/2}$ lines are higher than 710.8 eV, which strongly suggests that iron is present as Fe(III) species (Table 2). The second component of Fe 2p spectra exhibit even much higher BE (over 712 eV), which is not surprising, since many metal cations located in zeolites also exhibit higher binding energies comparing with their corresponding oxides [64–67]. This result is strongly affected by the degree of dispersion of cations as well as by the nature of their interaction with the zeolite matrix in which they are embedded. The higher BE for Fe(III) might reflect the occurrence of highly isolated species in this case. The areas of appropriate components in obtained zeolites change significantly from almost fifty-fifty to more than 60:40, which means that it depends on iron content.

3.4. Acidity of AlSiBEA and SiBEA determined by FTIR with CO adsorption

To determine the acidity of AlSiBEA and SiBEA supports the adsorption of CO as probe molecules has been performed. The CO adsorption experiments give information on Brønsted acidity related to OH groups as well as on the nature and strength of Lewis acidic sites related to Al atoms [68].

Difference spectra between FTIR spectra recorded after and before CO adsorption on AlSiBEA and SiBEA at 100 K are given in Fig. 8. As shown, the adsorption of CO at 100 K on AlSiBEA and SiBEA leads to the appearance of four main positive FTIR bands at 3645, 3595, 3440 and 3280 cm^{-1} and three negative bands at 3750, 3739 and 3715 cm^{-1}. The 3750, 3739 and 3715 cm^{-1} bands correspond to isolated external, isolated internal and terminal internal Si—OH located in vacant T-sites forming hydroxyl nests, in agreement with earlier report [34]. A very small shifts from 3739 to 3645 cm^{-1} (94 cm^{-1}) for isolated internal Si—OH groups and from 3715 to 3595 cm^{-1} (120 cm^{-1}) for terminal internal Si—OH groups indicate that both silanol groups have a very weak acidic character. The very low intensity of positive bands at 3440 and 3280 cm^{-1} for AlSiBEA and SiBEA (Fig. 8), related to red shifted bands of perturbed Al—OH and Si—O(H)—Al groups [26], suggests that only a small amount of both types of acidic hydroxyls groups occur in AlSiBEA and SiBEA. A large red shift of the band related to bridged Si—O(H)—Al groups from 3609 cm^{-1} to 3280 cm^{-1} ($\Delta\nu = 329\ cm^{-1}$) proves strong acidity of the proton of these groups. Moreover, the second FTIR band at 3440 cm^{-1} seems to be related to perturbed extra framework AlO—H groups (3668 cm^{-1}) ($\Delta\nu = 228\ cm^{-1}$), in agreement with recent work of Chakarova and Hadjiivanov [69].

3.5. Acidity of studied materials determined by TPD of NH_3

The strength and concentration of acidic sites in SiBEA, Fe_xSiBEA, AlSiBEA and Fe_xAlSiBEA have been determined by TPD of ammonia.

The TPD of NH_3 patterns of SiBEA, $Fe_{0.5}$SiBEA, $Fe_{1.0}$SiBEA, $Fe_{4.0}$SiBEA, AlSiBEA, $Fe_{0.5}$AlSiBEA, $Fe_{1.0}$AlSiBEA and $Fe_{4.0}$AlSiBEA are shown in Fig. 9. At least two unresolved maxima in the temperature range of 373–723 K occur. The first peak is centred at temperature range of 391–487 K, while the second one, much broader at about 530–640 K. It should be stressed here that introduction of iron by the postsynthesis method is accompanied by an increase in chemisorbed ammonia concentration from 94.3 $\mu mol\ g^{-1}$ (SiBEA) to 486.8 $\mu mol\ g^{-1}$ ($Fe_{1.0}$SiBEA). This effect results in a shift of NH_3 desorption peaks to higher temperatures.

Fe_xAlSiBEA are found to be significantly more acidic than Fe_xSiBEA. The TPD pattern of the AlSiBEA is spread in the temperature range of 373–673 K. Two clearly visible peaks are detected at about 433 and 553 K. Introduction of iron into the AlSiBEA sample has been resulted in a dramatic increase of acidic sites concentration from 194.7 $\mu mol\ g^{-1}$ (AlSiBEA) to 1408.3 $\mu mol\ g^{-1}$ ($Fe_{4.0}$AlSiBEA). Additionally, modification of AlSiBEA zeolite with iron shifts both peaks to higher temperatures are observed. However, this shift is more significant than for the Fe_xSiBEA. According to Jansen et al. [70] aluminium atoms in BEA zeolite are responsible for appearance of Brønsted acidic centres, present both on the internal and external surface as well as Lewis acidic centres that are

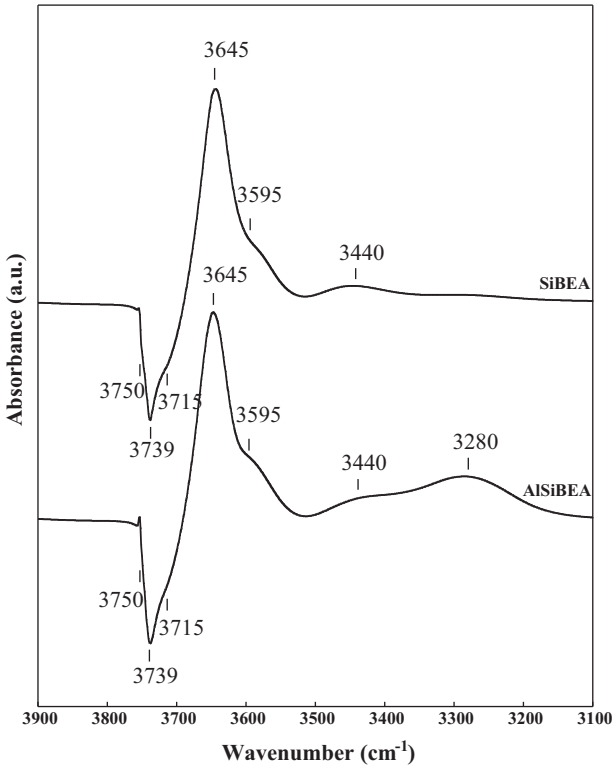

Fig. 8. Difference spectra between FTIR spectra recorded after and before CO adsorption on AlSiBEA and SiBEA at – 173 °C (CO in equilibrium).

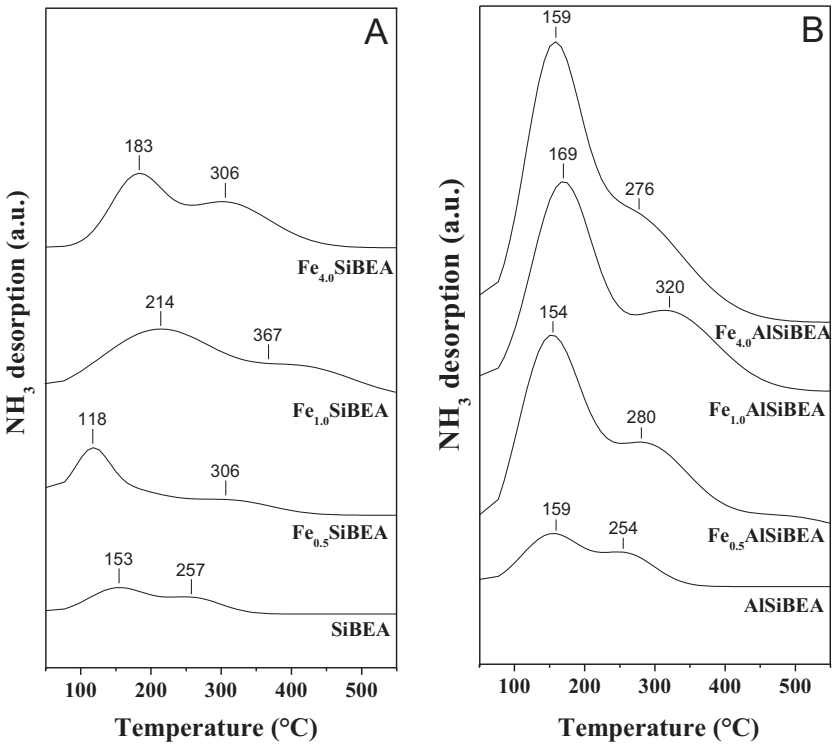

Fig. 9. TPD of NH_3 patterns of SiBEA, $Fe_{0.5}$SiBEA, $Fe_{1.0}$SiBEA, $Fe_{4.0}$SiBEA (A), and AlSiBEA, $Fe_{0.5}$AlSiBEA, $Fe_{1.0}$AlSiBEA, $Fe_{4.0}$AlSiBEA (B).

associated to local defects. Camiloti et al. [71] have discussed the presence of two types of acidic centres in the iron containing BEA zeolites. According to these results the first peak can be attributed to desorption of ammonia from Lewis acidic centres, while the second one present at higher temperature can be related to ammonia desorbing from Brønsted acidic centres.

3.6. Catalytic activity

Fe_xAlSiBEA and Fe_xSiBEA are used as catalysts for N_2O decomposition and SCR of NO with ammonia. Fig. 10 presents the results of the catalytic tests in the process of N_2O decomposition to nitrogen and oxygen. The reaction starts at about 553 K and N_2O conversion increases with an increasing of reaction temperature. The catalytic activity of the samples without iron (SiBEA, AlSiBEA) is poor and N_2O conversion is below 10% in whole temperature range. Introduction of iron into these samples results in significant increasing of their activity in the process of N_2O decomposition. However, various effects of iron content on catalytic performance are observed for both Fe_xAlSiBEA and Fe_xSiBEA. The $Fe_{1.0}$SiBEA and $Fe_{1.0}$AlSiBEA are much more active than SiBEA and AlSiBEA. Therefore, iron seems to play an important role in the process of N_2O decomposition. An increasing of iron content up to 4.0 wt.% influences activity of Fe_xAlSiBEA and Fe_xSiBEA in different ways. For Fe_xAlSiBEA, an increase in iron content leads to increase of activity (~100% N_2O conversion at 753 K for $Fe_{4.0}$AlSiBEA), while an opposite effect was observed for Fe_xSiBEA, where the sample with lower content of iron ($Fe_{1.0}$SiBEA) is slightly more active than $Fe_{4.0}$SiBEA with much higher content of iron. This effect could be explained by the presence of different iron species in these samples. For $Fe_{1.0}$SiBEA, iron is mainly present in the framework as pseudo-tetrahedral Fe(III) (Fig. 4), while for $Fe_{4.0}$SiBEA, beside dominant pseudo-tetrahedral Fe(III), octahedral extra-framework Fe(III) are also evidenced by DR UV–vis, XPS and EXAFS.

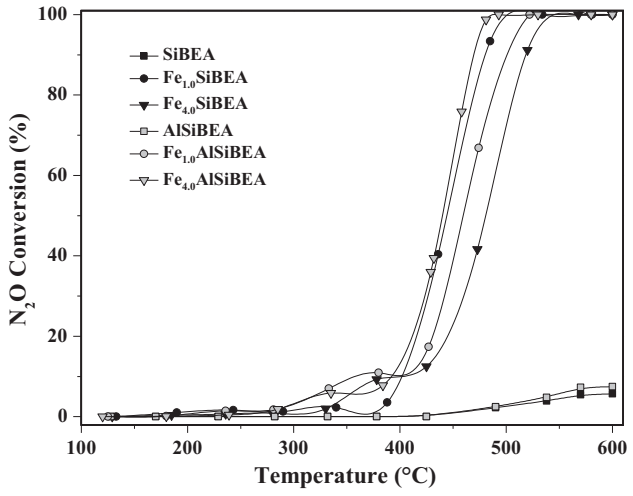

Fig. 10. N_2O conversion in N_2O decomposition on SiBEA, $Fe_{1.0}$SiBEA, $Fe_{4.0}$SiBEA, AlSiBEA, $Fe_{1.0}$AlSiBEA and $Fe_{4.0}$AlSiBEA.

Therefore, it seems that framework pseudo-tetrahedral Fe(III), which are observed in $Fe_{1.0}$SiBEA are responsible for high activity of this catalyst in N_2O decomposition. The results of catalytic tests obtained for $Fe_{1.0}$SiBEA and $Fe_{1.0}$AlSiBEA show that high activity does not necessarily depend on the presence of extra-framework Fe species, as it was postulated earlier [72,73].

Moreover, acidity, which is different for both series of the samples, is a possible factor influencing their catalytic activity in N_2O decomposition. The differences in acidity of the catalysts are related to the presence of Al and Fe atoms in the zeolite structure, which can act simultaneously as Brønsted (bridging OH groups in ≡Al(III)—O(H)—Si≡ or ≡Fe(III)—O(H)—Si≡) and Lewis (unsaturated Al and Fe framework atoms) acidic centres and influence catalytic properties of the Fe_xAlSiBEA and Fe_xSiBEA. The active centres for Fe_xAlSiBEA are probably related to bridged ≡Al(III)—O(H)—Si≡ groups with a very strong acidic character, as evidenced by FTIR

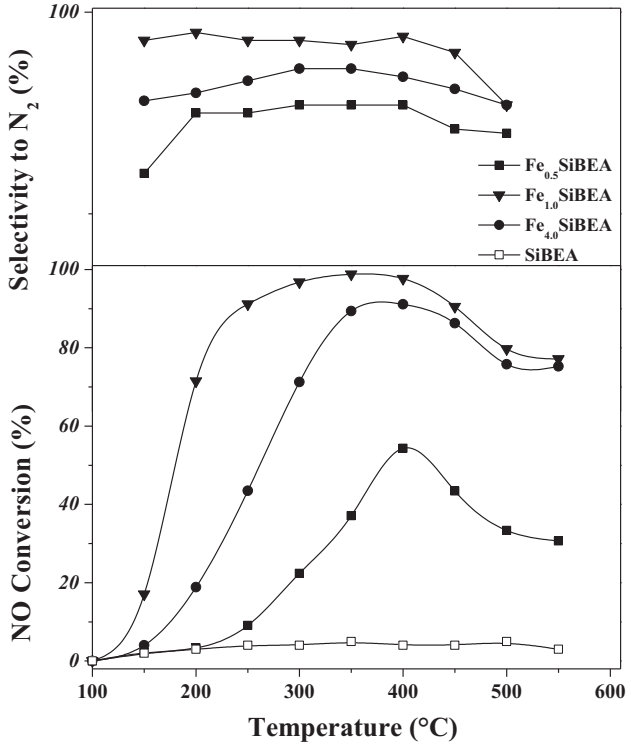

Fig. 11. NO conversion and N_2 selectivity in SCR of NO with NH_3 on SiBEA, $Fe_{0.5}$SiBEA, $Fe_{1.0}$SiBEA, $Fe_{4.0}$SiBEA.

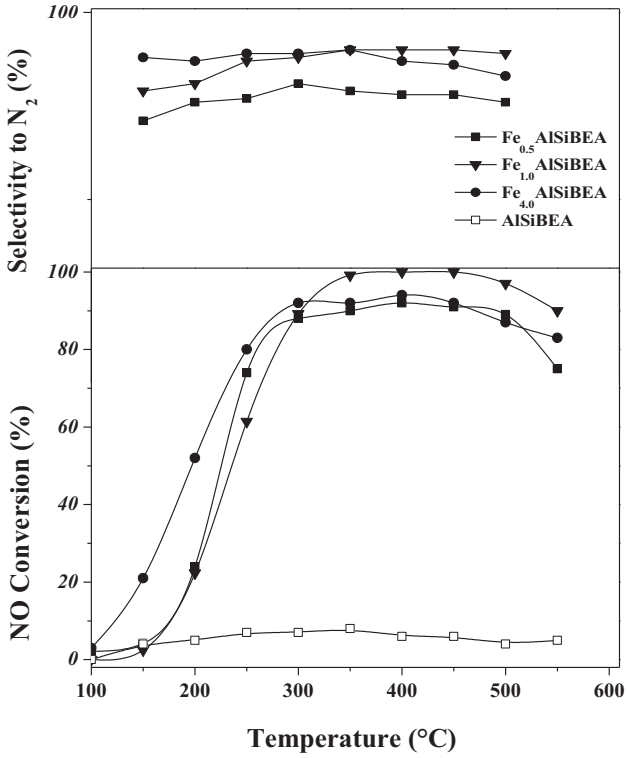

Fig. 12. NO conversion and N_2 selectivity in SCR of NO with NH_3 on AlSiBEA, $Fe_{0.5}$AlSiBEA, $Fe_{1.0}$AlSiBEA and $Fe_{4.0}$AlSiBEA.

of adsorbed CO. It strongly influences of the catalytic activity of $Fe_{4.0}$AlSiBEA. For Fe_xSiBEA, N_2O conversion may be related to the presence of framework pseudo-tetrahedral sites such as ≡Fe(III)—O(H)—Si≡. As it was reported [26], these centres are only slightly less acidic than the corresponding ≡Al(III)—O(H)—Si≡ analogue. Therefore, it could be suggested that the higher strength and concentration of acidic centres (≡Al(III)—O(H)—Si≡) in $Fe_{4.0}$AlSiBEA comparing to $Fe_{4.0}$SiBEA catalyst is responsible for its higher activity in the N_2O decomposition, what is in line with earlier studies [72]. It should be noted here that iron containing zeolite materials (Fe_xSiBEA and Fe_xAlSiBEA) prepared by post-synthesis method can be considered as effective catalysts in N_2O decomposition process. Their catalytic activity (~ 100% N_2O conversion above 790 K for all samples) is close to the value of the parameter measured for FeZSM-5, obtained using CVD method (~100% N_2O conversion at 770 K) [29].

Fe_xSiBEA and Fe_xAlSiBEA have also been tested as catalysts in the SCR of NO with ammonia. N_2 and N_2O are the only detected nitrogen-containing reaction products. The results of the studies performed for both series of catalysts are presented in Figs. 11 and 12 respectively. As shown earlier [43], the catalytic activity of the samples without iron (SiBEA, AlSiBEA) is very poor and NO conversion is below 10% at whole temperature range. The NO conversion substantially increases after incorporation of a little amount of iron in the framework of SiBEA and AlSiBEA zeolite as pseudo-tetrahedral Fe(III) species, as shown for $Fe_{0.5}$SiBEA (Fig. 11) and $Fe_{0.5}$AlSiBEA (Fig. 12). It suggests that pseudo-tetrahedral Fe(III) species are responsible for high activity of both catalysts in SCR of NO process. The activity of Fe_xSiBEA and Fe_xAlSiBEA increases after introduction of a larger amounts of iron (1.0 and 4.0 Fe wt.%) (Figs. 11 and 12).

The various effects of iron content on the catalytic performance are observed for Fe_xAlSiBEA and Fe_xSiBEA. The NO conversion increases to about 673 K reaching 55% for $Fe_{0.5}$SiBEA, while at higher temperature the NO conversion decreases probably due to the side process of direct ammonia oxidation. The $Fe_{1.0}$SiBEA shows much higher activity (above 96% of NO conversion with the selectivity to N_2 about 90% at 573 K) and less significant effect of direct ammonia oxidation in the high temperature range. An increase in iron content up to 4 wt.% ($Fe_{4.0}$SiBEA) results in decreasing of the catalytic activity (above 70% of NO conversion with a selectivity to N_2 about 80% at 573 K). This effect could be explained by the different state of iron present in Fe_xSiBEA and Fe_xAlSiBEA. It seems that the highest conversion of NO measured over $Fe_{1.0}$SiBEA is related to the presence of isolated pseudo-tetrahedral Fe(III) in the zeolite framework (evidenced by DR UV–vis, XANES and EXAFS) [5,74,75].

The $Fe_{4.0}$SiBEA sample containing framework pseudo-tetrahedral and extra-framework octahedral Fe(III) species is less active in the SCR of NO process than $Fe_{1.0}$SiBEA (Fig. 11). Fe_xAlSiBEA presents much better catalytic activity in SCR of NO with ammonia process. This series shows high activity (above 85% of NO conversion) in a broad temperature range of 523–773 K. Additionally, for Fe_xAlSiBEA the effect of direct ammonia oxidation is less significant than for Fe_xSiBEA. It should be noted that a commercial catalysts for this process, based on V_2O_5–TiO_2 oxide system, operate in a significantly narrower temperature range of 523–673 K [5]. Therefore, these preliminary results obtained in our studies, especially for Fe_xAlSiBEA, are very promising. It is seen that the $Fe_{4.0}$AlSiBEA catalyst gives higher NO conversion almost in the whole temperature range from 523 to 773 K and is more selective towards N_2 than $Fe_{4.0}$SiBEA. Iwasaki et al. [27] have studied catalytic performance of Fe/ZSM-5 materials prepared by several methods (Imp, RSIE, CVD). They have suggest that iron-containing ZSM-5 catalysts demonstrate high activity in SCR-NO when iron is introduced by CVD method (~100% NO conversion at about 573 K). The similar results have been reported by Delahay et al. [28]. It should be noted that nitrogen oxide conversions measured for $Fe_{1.0}$SiBEA (>90% NO conversion at 523 K) and $Fe_{1.0}$AlSiBEA (>90% NO conversion at 573 K) proves their high catalytic activity in SCR-NO with ammonia. Therefore, not only CVD but also post-synthesis

method leads to obtain well-define catalysts, containing Fe^{3+} ions in pseudo-tetrahedral coordination. It suggests that isolated Fe sites play major role in SCR-NO reaction, as evidenced earlier [12,76].

It clearly indicates that the active centres involved in both cases are not the same. Another important parameter is acidity, which is significantly larger for Fe_xAlSiBEA than for Fe_xSiBEA. It is well known that acidic centres play an important role in the SCR of NO process and they are responsible for chemisorption and activation of ammonia molecules [5]. Therefore, apart from different forms of iron species also acidity strongly influences the catalytic performance of the studied samples. As evidenced by low-temperature CO adsorption studies, the ≡Al(III)—O(H)—Si≡ sites, identified in Fe_xAlSiBEA, probably play an important role in the catalytic activity of these catalysts. In case of Fe_xSiBEA, the active centres are probably related to the presence of framework pseudo-tetrahedral ≡Fe(III)—O(H)—Si≡ sites. However, these centres are less acidic than ≡Al(III)—O(H)—Si≡ ones. Thus, the catalytic activity of Fe_xAlSiBEA and Fe_xSiBEA in the SCR of NO process seems to be related to the presence of isolated pseudo-tetrahedral iron species. Moreover, the higher strength and concentration of acidic centres in $Fe_{1.0}$AlSiBEA than in $Fe_{1.0}$SiBEA (evidenced by FTIR of adsorbed CO and TPD of NH_3) seem to be responsible for its higher catalytic activity. It is in line with the report of Schwidder et al. [77] who have suggested that activity of the catalysts in the SCR of NO process depends on their acidity.

Comparison of the results physicochemical characterization (DR UV–vis, EXAFS, XANES, XPS and FTIR-CO) and results of the catalytic tests clearly shows that catalysts acidity has influenced catalytic activity of studied materials.

4. Conclusions

Two-steps postsynthesis modification of BEA zeolite results in the incorporation of iron into vacant T-atom sites of the zeolite framework as pseudo-tetrahedral Fe(III) species, what was evidenced by combined used of XRD, DR UV–vis, XAS, ^{57}Fe Mössbauer and XPS investigations.

Fe_xAlSiBEA and Fe_xSiBEA have been found to be active and selective catalysts of N_2O decomposition as well as of SCR of NO with ammonia. Their catalytic activity strongly depends on the speciation and amount of introduced iron species into zeolite structure as well as their acidity. The presence of extra-framework octahedral Fe(III) results in the less effective catalytic system. Therefore, it seems that these iron species are less catalytically active than framework pseudo-tetrahedral Fe(III).

The framework pseudo-tetrahedral Fe(III) are mainly observed in the catalysts with low iron content ($Fe_{0.5}$AlSiBEA, $Fe_{1.0}$AlSiBEA, $Fe_{0.5}$SiBEA and $Fe_{1.0}$SiBEA). Such species are a result of incorporation of Fe(III) ions into vacant T-atom sites of SiBEA.

In contrast, for the catalysts with higher iron content ($Fe_{4.0}$AlSiBEA, $Fe_{4.0}$SiBEA) besides framework pseudo-tetrahedral Fe(III), which are main species, extra-framework octahedral Fe(III) occur.

The framework pseudo-tetrahedral ≡Al(III)—O(H)—Si≡ and ≡Fe(III)—O(H)—Si≡ sites have influenced the catalytic properties of the obtained catalysts. The higher strength and concentration of acidic centres in Fe_xAlSiBEA comparing to Fe_xSiBEA seems to be responsible for their higher activity in the SCR of NO process and much higher selectivity towards N_2.

Acknowledgements

The presented studies were performed in the frame of GDRI programme. Part of the research was done with equipment purchased in the frame of European Regional Development Fund (Polish Innovation Economy Operational Programme – contract no. POIG.02.01.00-12-023/08).

Appendix A. Supplementary data

Supplementary data associated with this article can be found, in the online version, at http://dx.doi.org/10.1016/j.apcatb.2013.03.022.

References

[1] I. Hnat, I. Kocemba, J. Rynkowski, T. Onfroy, S. Dzwigaj, Catalysis Today 176 (2011) 229.
[2] S. Dzwigaj, M.J. Peltre, P. Massiani, A. Davidson, M. Che, T. Sen, S. Sivasanker, Chemical Communications (1998) 87.
[3] J. Perez-Ramirez, F. Kapteijn, G. Mul, J.A. Moulijn, Applied Catalysis B 35 (2002) 227.
[4] J. Perez-Ramirez, F. Kapteijn, G. Mul, J.A. Moulijn, Chemical Communications (2001) 693.
[5] G. Busca, L. Lietti, G. Ramis, F. Berti, Applied Catalysis B 18 (1998) 1.
[6] F. Kapteijn, J. Rodríguez-Mirasol, J.A. Moulijn, Applied Catalysis B 9 (1996) 25.
[7] E.V. Kondratenko, R. Kraehnert, J. Radnik, M. Baerns, J. Perez-Ramirez, Applied Catalysis B 298 (2006) 73.
[8] J. Oi, A. Obuchi, G.R. Bamwenda, A. Ogata, H. Yagita, S. Kushiyama, K. Mizuno, Applied Catalysis B 12 (1997) 277.
[9] K. Doi, Y. Wu, R. Takeda, A. Matsunami, N. Arai, T. Tagawa, S. Goto, Applied Catalysis B 35 (2001) 43.
[10] J. Haber, M. Nattich, T. Machej, Applied Catalysis B 77 (2008) 278.
[11] S. Tanaka, K. Yuzaki, S. Ito, H. Uetsuka, S. Kameoka, K. Kunimori, Catalysis Today 63 (2000) 413.
[12] R.Q. Long, R.T. Yang, Journal of the American Chemical Society 121 (1999) 5595.
[13] A. Ma, W. Grunert, Chemical Communications (1999) 71.
[14] S. Sklenak, P. Andrikopoulos, B. Boekfa, B. Jansang, J. Novakova, L. Benco, T. Bucko, J. Hafner, J. Dedecek, Z. Sobalik, Journal of Catalysis 272 (2010) 262.
[15] E. Kondratenko, V. Kondratenko, M. Santiago, J. Perez-Ramirez, Journal of Catalysis 256 (2008) 248.
[16] G. Delahay, M. Mauvezin, A. Guzman-Vargas, B. Coq, Catalysis Communications 3 (2002) 385.
[17] K. Sun, H. Xia, E. Hensen, R. van Santen, C. Li, Journal of Catalysis 238 (2006) 186.
[18] G. Pirngruber, Journal of Catalysis 219 (2003) 456.
[19] P. Roy, R. Prins, G. Pirngruber, Applied Catalysis B 80 (2008) 226.
[20] J. Perez-Ramirez, F. Kapteijn, K. Schöffel, J.A. Moulijn, Applied Catalysis B 44 (2003) 117.
[21] B. Coq, M. Mauvezin, G. Delahay, S. Kieger, Journal of Catalysis 195 (2000) 298.
[22] S. Dzwigaj, L. Stievano, F. Wagner, Michel Che, Journal of Physical Chemistry 68 (2007) 1885.
[23] J. Janas, S. Dzwigaj, Catalysis Today 176 (2011) 272.
[24] S. Dzwigaj, J. Janas, W. Rojek, L. Stievano, F. Wagner, F. Averseng, M. Che, Applied Catalysis B 86 (2009) 45.
[25] J. Janas, J. Gurgul, R. Socha, T. Shishido, M. Che, S. Dzwigaj, Applied Catalysis B 91 (2009) 113.
[26] K. Hadjiivanov, E. Ivanova, R. Kefirov, J. Janas, A. Plesniar, S. Dzwigaj, M. Che, Microporous and Mesoporous Materials 131 (2010) 1.
[27] M. Iwasaki, K. Yamazaki, K. Banno, H. Shinjoh, Journal of Catalysis 260 (2008) 205.
[28] G. Delahay, D. Valade, A. Guzman-Vargas, B. Coq, Applied Catalysis B 55 (2005) 149.
[29] G. Pirngruber, M. Luechinger, P. Roy, A. Cecchetto, P. Smirniotis, Journal of Catalysis 224 (2004) 429.
[30] E.J.M. Hensen, Q. Zhu, R.A. van Santen, Journal of Catalysis 220 (2003) 260.
[31] A.H. Øygarden, J.P. Pérez-Ramírez, Applied Catalysis B 65 (2006) 163.
[32] G.J. Long, T.E. Cranshaw, G. Longworth, Mössbauer Effect Reference and Data Journal 6 (1983) 42.
[33] D.G. Rancourt, J.Y. Ping, Nuclear Instruments and Methods in Physics Research Section B 58 (1991) 85.
[34] M. Camblor, A. Corma, J. Perez-Pariente, Journal of the Chemical Society, Chemical Communications (1993) 557.
[35] S. Dzwigaj, P. Massiani, A. Davidson, M. Che, Journal of Molecular Catalysis 155 (2000) 169.
[36] S. Dzwigaj, T. Shishido, Journal of Physical Chemistry C 112 (2008) 5803.
[37] H. Tippins, Physical Review B 72 (1970) 279.
[38] S. Bordiga, R. Buzzoni, F. Geobaldo, C. Lamberti, E. Giamello, A. Zecchina, G. Leofanti, G. Petrini, G. Tozzola, G. Vlaic, Journal of Catalysis 158 (1996) 486.
[39] P. Wu, T. Komatsu, T. Yashima, Microporous and Mesoporous Materials 20 (1998) 139.
[40] L. Capek, V. Kreibich, J. Dedecek, T. Grygar, B. Wichterlova, Z. Sobalik, J.A. Martens, R. Brosius, V. Tokarova, Microporous and Mesoporous Materials 80 (2005) 279.
[41] J. Perez-Ramirez, J.C. Groen, A. Brückner, M.S. Kumar, U. Bentrup, M.N. Debbagh, L.A. Villaescusa, Journal of Catalysis 232 (2005) 318.

[42] P. Balle, B. Geiger, S. Kureti, Applied Catalysis B 85 (2008) 109.
[43] J. Janas, T. Machej, J. Gurgul, R.P. Socha, M. Che, S. Dzwigaj, Applied Catalysis B 75 (2007) 239.
[44] J.H. Choy, J.B. Yoon, D.K. Kim, S.H. Hwang, Inorganic Chemistry 34 (1995) 6524.
[45] T.E. Westre, P. Kennepohl, J.G. de Witt, B. Hedman, K.O. Hodgson, E.I. Solomon, Journal of the American Chemical Society 119 (1997) 6297.
[46] J. Gurgul, K. Łątka, I. Hnat, J. Rynkowski, S. Dzwigaj, Microporous and Mesoporous Materials 168 (2013) 1.
[47] P. Fejes, K. Lázár, I. Marsi, A. Rockenbauer, L. Korecz, J.B. Nagy, S. Perathoner, G. Centi, Applied Catalysis A 252 (2003) 75.
[48] R.M. Mihályi, K. Lázár, M. Kollár, F. Lónyi, G. Pál-Borbély, Á. Szegedi, Microporous and Mesoporous Materials 110 (2008) 51.
[49] M.S. Kumar, M. Schwidder, W. Grünert, U. Bentrup, A. Brückner, Journal of Catalysis 239 (2006) 173.
[50] K. Arishtirova, P. Kovacheva, A. Predoeva, Applied Catalysis A 243 (2003) 191.
[51] P. Kovacheva, K. Arishtirova, A. Predoeva, Reaction Kinetics and Catalysis Letters 79 (2003) 149.
[52] L.P. Oleksenko, Theoretical and Experimental Chemistry 40 (2004) 331.
[53] W. Grünert, R. Schlögl, Molecular Sieves 4 (2004) 467.
[54] J. Janas, J. Gurgul, R.P. Socha, S. Dzwigaj, Applied Catalysis B 91 (2009) 217.
[55] K. Nomura, Y. Ujihira, A. Vértes, Journal of Radioanalytical and Nuclear Chemistry 202 (1996) 103.
[56] M. Descostes, F. Mercier, N. Thromat, C. Beaucaire, M. Gautier-Soyer, Applied Surface Science 165 (2000) 288.
[57] T.-C. Lin, G. Seshadri, J.A. Kelber, Applied Surface Science 119 (1997) 83.
[58] T. Yamashita, P. Hayes, Applied Surface Science 254 (2008) 2441.
[59] P.C.J. Graat, M.A.J. Somers, Applied Surface Science 100/101 (1996) 36.
[60] Th. Schedel-Niedrig, W. Weiss, R. Schlögl, Physical Review B 52 (1995) 17449.
[61] B.L. Maschhoff, N.R. Armstrong, Langmuir 7 (1991) 693.
[62] M. Muhler, R. Schlögl, G. Ertl, Journal of Catalysis 138 (1992) 413.
[63] Y. Okamoto, M. Fujii, T. Imanaka, S. Teranishi, Bulletin of the Chemical Society of Japan 48 (1975) 1163.
[64] K.M. Minachev, G.V. Antoshin, E.S. Shpiro, Akademiia nauk SSSR. Izvestiia. Seriia khimicheskaia (1974) 1012.
[65] K.M. Minachev, G.V. Antoshin, E.S. Shpiro, Y.A. jusiphov, Proc. 1st All-union Conf. Zeolites in Catalysis, Academy of Sciences of the USSR, Novosibirsk, 1976.
[66] B. Wichterlova, L. Krajicikova, Z. Tvruzkova, S. Beran, Journal of the Chemical Society, Faraday Transactions 1 80 (1984) 2639.
[67] K. Yogo, S. Tanaka, T. Ono, T. Mikami, E. Kikuchi, Microporous Materials 3 (1994) 39.
[68] K. Hadjiivanov, G.N. Vayssilov, Advances in Catalysis 47 (2002) 307.
[69] K. Chakarova, K. Hadjiivanov, Journal of Physical Chemistry C 115 (2011) 4806.
[70] J. Jansen, E. Creyghton, S. Njo, H. van Koningsveld, H. van Bekkum, Catalysis Today 38 (1997) 205.
[71] A. Camiloti, S. Jahn, N. Velasco, L. Moura, D. Cardoso, Applied Catalysis A 182 (1999) 107.
[72] J. Pérez-Ramírez, F. Kapteijn, J.C. Groen, A. Domenech, G. Mul, J.A. Moulijn, Journal of Catalysis 214 (2003) 33.
[73] J. Perez-Ramirez, Journal of Catalysis 227 (2004) 512.
[74] R. Long, R. Yang, Catalysis Letters 74 (2001) 201.
[75] H. Bosch, F. Janssen, Catalysis Today 2 (1988) 369.
[76] M. Schwidder, M.S. Kumar, K. Klementiev, M.M. Pohl, A. Brückner, W. Grünert, Journal of Catalysis 231 (2005) 314.
[77] M. Schwidder, M. Kumar, U. Bentrup, J. Perez-Ramirez, A. Bruckner, W. Grunert, Microporous and Mesoporous Materials 111 (2008) 124.